Spatial representativeness and uncertainty of eddy covariance carbon flux measurements for upscaling net ecosystem productivity to the grid scale

Youhua Ran[1,2], Xin Li[1,3], Rui Sun[4,5], Natascha Kljun[6], Lei Zhang[4,5], Xufeng Wang[1], Gaofeng Zhu[7]

1. Key Laboratory of Remote Sensing of Gansu Province, Heihe Remote Sensing Experimental Research Station, Cold and Arid Regions Environmental and Engineering Research Institute, Chinese Academy of Sciences, Lanzhou 730000, China

2. University of Chinese Academy of Sciences, Beijing 100049, China

3. CAS Center for Excellence in Tibetan Plateau Earth Sciences, Beijing 100101, China

4. State Key Laboratory of Remote Sensing Science, Jointly Sponsored by Beijing Normal University and the Institute of Remote Sensing Applications, CAS, Beijing 100875, China

5. School of Geography and Remote Sensing Sciences, Beijing Normal University, Beijing 100875, China

6. Department of Geography, Swansea University, Swansea SA2 8PP, U.K.

7. Key Laboratory of Western China's Environmental Systems, Lanzhou University, Lanzhou 730000, China

Corresponding author and address:

Youhua Ran
Cold and Arid Regions Environmental and Engineering Research Institute,
Chinese Academy of Sciences
320 West Donggang Road, Lanzhou 730000, Gansu Province, China
Email: ranyh@lzb.ac.cn
Phone: +86-931-4967964

Agricultural and Forest Meteorology, accepted 09 May 2016

Abstract:

Eddy covariance (EC) measurements are often used to validate net ecosystem productivity (NEP) estimated from satellite remote sensing data and biogeochemical models. However, EC measurements represent an integrated flux over their footprint area, which usually differs from respective model grids or remote sensing pixels. Quantifying the uncertainties of scale mismatch associated with gridded flux estimates by upscaling single EC tower NEP measurements to the grid scale is an important but not yet fully investigated issue due to limited data availability as well as knowledge of flux variability at the grid scale. The Heihe Watershed Allied Telemetry Experimental Research (HiWATER) Multi-Scale Observation Experiment on Evapotranspiration (MUSOEXE) built a flux observation matrix that includes 17 EC towers within a 5 km × 5 km area in a heterogeneous agricultural landscape in northwestern China, providing an unprecedented opportunity to evaluate the uncertainty of upscaling due to spatial representative differences at the grid scale. Based on the HiWATER-MUSOEXE data, this study evaluated the spatial representativeness and uncertainty of EC CO_2 flux measurements for upscaling to the grid scale using a scheme that combines a footprint model and a model-data fusion method. The results revealed the large spatial variability of gross primary productivity (GPP), ecosystem respiration (Re), and NEP within the study site during the growing season from 10 June to 14 September 2012. The variability of fluxes led to high variability in the representativeness of single EC towers for grid-scale NEP. The systematic underestimations of a single EC tower may reach 92(±11)%, 30(±11)%, and 165(±150)% and the overestimations may reach 25(±14)%, 20(±13)%, and 40(±33)% for GPP, Re, and NEP, respectively. This finding suggests that remotely sensed NEP at the global scale (e.g., MODIS products) should not be validated against single EC tower data in the case of heterogeneous surfaces. Any systematic bias should be addressed before upscaling EC data to grid scale. Otherwise, most of the systematic bias may be propagated to grid scale due to the scale dependence of model parameters. A systematic bias greater than 20% of the EC measurements can be corrected effectively using four indicators proposed in this study. These results will contribute to the understanding of spatial representativeness of EC towers within a heterogeneous landscape, to upscaling carbon fluxes from the footprint to the grid scale, to the selection of the location of EC towers, and to the reduction in the bias of NEP products by using an improved parameterization scheme of remote-sensing driven models, such as VPRM.

Key words： Ecosystem fluxes; Scale dependence; Remote sensing; Heterogeneous agricultural landscape; Footprint model

Spatial representativeness and uncertainty of eddy covariance carbon flux measurements for upscaling net ecosystem productivity to the grid scale

1 Introduction

Carbon dioxide, as an important greenhouse gas, plays a vital role in regulating the Earth's surface temperature through radiative forcing and the greenhouse effect. Atmosphere carbon dioxide has increased by ~40% since 1750 (Ballantyne et al., 2012), with a pronounced increase in the past ten years (IPCC, 2013). Vegetation productivity is one of the main sinks of atmospheric CO_2. Net ecosystem production (NEP) is the net rate of carbon accumulation within an ecosystem. It is defined as the difference between the amount of carbon (C) removed from the atmosphere in the form of carbon dioxide through photosynthesis and the loss of carbon through the respiration of vegetation and soil. The quantification of NEP indicates whether an ecosystem is a net sink or source of atmospheric CO_2. Positive NEP indicates the ecosystem is a carbon sink, while negative NEP indicates the ecosystem is a carbon source.

Eddy covariance (EC) instruments, remote sensing-based models, and biogeochemical models are three main methods to quantify the NEP of terrestrial ecosystems. The EC technique is considered one of the most direct and appropriate ways to measure and calculate turbulent fluxes of CO_2 on a local scale (Burba, 2013; Wang et al., 2015). Remote sensing-based models, on the other hand, provide quantitative estimates of spatially continuous NEP, which can be used to evaluate the spatial patterns and seasonal to inter-annual variability of carbon sources/sinks (Kimball et al., 2009; Sasai et al., 2011). However, remote sensing is an indirect measurement and is associated with large uncertainty (Chasmer et al., 2009; Coops et al., 2007; Kwon and Larsen, 2012; Turner et al., 2006; Zhang et al., 2012). Biogeochemical models use process understanding obtained from past measurements within ecosystems to predict future ecosystem dynamics given a range of different driving mechanisms and contributing factors. Model uncertainty often varies as a result of model structure, boundary conditions, and parameterization schemes (Huntzinger et al., 2012; Mitchell et al., 2009; Randerson et al., 2009). Currently, EC measurements are important for both the calibration and validation of NEP estimated using biogeochemical models and those driven using remote sensing data (Heinsch et al., 2006; Luo et al., 2011; Raupach et al., 2005; Verma et al., 2014; Wang et al., 2009; Weng et al., 2011). However, EC measurements represent an integrated flux over their footprint area, which may not match the scale of the respective model grids or remote sensing pixels. It is therefore important to address the potential uncertainty related to spatial and temporal scaling as this may significantly alter the suitability of EC tower data for the evaluation and calibration of estimates derived from remotely sensed data and biogeochemical models (Göckede et al., 2008, 2010).

Errors in EC observations can be decomposed into measurement error and representativeness error (Lasslop et al., 2008; Li, 2014; Raupach et al., 2005). In general, part of measurement errors can be minimized by calibrating instruments and by data processing techniques such as averaging flux values (Wang et al., 2015), while representativeness error may be dominant at a grid scale (Chasmer et al., 2009; Raupach et al., 2005). We therefore focus on representativeness error in this study. Here, the representativeness error of the EC measurements is relative to the grid scale. The representativeness error is affected by measurement height, surface roughness and thermal stability associated with the heterogeneity of vegetation structural and disturbance patterns (Burba, 2001; Chasmer et al., 2011; Chen et al., 2009; Göckede et al., 2010; Raupach et al., 2005). EC systems are usually set up within relatively homogeneous ecosystems, where the spatial variability of the vegetation structural characteristics is minimal to reduce uncertainty. However, heterogeneity is inevitable within complex and fragmented landscapes, such as those found in semi-arid

agro-ecosystems in western China.

The spatial representativeness of EC flux measurements at the grid scale in complex and fragmented landscapes is still not completely understood, mainly due to limited available EC data within the grid area. The related studies are rather limited and most of them are based on single tower data. For example, Barcza et al. (2009) quantified the spatial representativeness of tall tower-based EC measurements at a height of 82 m within a heterogeneous landscape by combining footprint analysis and land cover classification. These authors found that the source region distribution of fluxes was very similar from year to year. This means that the spatial representativeness is temporally stable. Chasmer et al. (2009) proposed a method to derive the spatial representativeness of EC measurements relative to a 1-km resolution from the Moderate Resolution Imaging Spectroradiometer (MODIS) pixel using a structure-based gross primary production (GPP) model. In addition, Chasmer et al. (2011) examined the relationship between the spatial frequency of the 3-D vegetation attributes within the MODIS pixel and the EC footprint, and found that the comparability of the flux data obtained from the EC measurements and the MODIS pixel may depend on the relationship of the vegetation structure. Further, Xiao et al. (2011) estimated parameters for upscaling the EC flux to a regional scale using a single EC tower and found that the model parameters estimated from a single site are not representative of the parameter values for a given plant functional type. This means that parameter heterogeneity exists within plant functional types defined at a coarse scale. Consequently, plant functional types need to be defined at a fine resolution, and the associated spatial representativeness of EC flux measurements should be evaluated. The above-mentioned studies have touched on some key aspects for evaluating the spatial representativeness or representativeness error of EC flux measurements, and provide an important basis for more detailed research. Their main limitation is that they are based on strong underlying assumptions and few measurements, which reduces the reliability of the conclusions drawn.

An extensive grid-based flux matrix was constructed in a fragmented agro-ecosystem in western China as part of the Heihe Watershed Allied Telemetry Experimental Research (HiWATER)--Multi-Scale Observation Experiment on Evapotranspiration (MUSOEXE) over a heterogeneous land surface (Li et al., 2013; Liu et al., 2016). This constitutes a component of the integrated study of the water-ecosystem-economy in the Heihe River Basin (Cheng et al., 2014). Compared with previous campaigns, such as BOREAS (Boreal Ecosystem-Atmosphere Study) (Sellers et al., 1995), CASES-99 (Cooperative Atmosphere-Surface Exchange Study-1999) (Poulos et al., 2002), SGP97 (Southern Great Plains-1997) (Twine et al., 2000), IHOP 2002 (International H2O Project) (Weckwerth et al., 2004), LITFASS-2003 (Lindenberg Inhomogeneous Terrain-Fluxes between Atmosphere and Surface: a long-term study) (Beyrich and Mengelkamp, 2006), and BEAREX-08 (Bushland Evapotranspiration and Agricultural Remote Sensing Experiment-2008) (Anderson et al., 2012), the flux matrix of HiWATER-MUSOEXE includes 17 EC towers within a 5 km×5 km area and thus provides the first opportunity to evaluate the representativeness of the towers with respect to grid-scale carbon fluxes. The grid-based tower setup can be used to reveal the spatial heterogeneities of carbon fluxes, to determine scaling effects and to provide ground truth data for the improvement of remote sensing-based models and scaling approaches for carbon fluxes over heterogeneous land surfaces.

The goals of this study are to use an EC grid-based deployment methodology to quantify the uncertainty of grid-scale NEP estimation resulting from the representativeness of a single EC tower and to explore the tools that can reduce this uncertainty. The specific objectives are to (1) evaluate the representativeness of single tower data for long-term grid-scale carbon flux estimates; (2) assess the influence of the representativeness of a heterogeneous vegetation structure within the EC footprint on NEP at the grid scale; and (3) explore the uncertainty of the representativeness for upscaling NEP flux tower data to the grid scale using a model-data fusion method. The findings of this study will contribute to an understanding of the spatial representativeness of EC towers within a heterogeneous landscape for upscaling carbon fluxes from the footprint to the grid scale, to the site selection for the location of EC towers, and to the validation and improvement of NEP modeling.

2 Study sites and data

2.1 Site description

The HiWATER-MUSOEXE flux matrix was established in the Zhangye oasis in the central reach of the Heihe River Basin. The Zhangye oasis is located in the central part of the Hexi corridor in the arid region of northwestern China (Figure 1). This region has an arid continental climate, and the mean annual temperature is approximately 7 ºC. The mean annual precipitation is 117 mm, with distinct seasonal variation, and the mean annual potential evaporation is 2390 mm (Li and Zhao, 2010). This agro-ecosystem is dependent on irrigation. The irrigation water is mainly sourced from the Heihe River and groundwater. In 2006, the exploitation of groundwater was 3.59×10^8 m^3, of which 3.06×10^8 m^3 was used for agricultural irrigation. The core experimental area of HiWATER-MUSOEXE is nearly flat. The main soil texture is silt (67.67%) and the mean organic matter content is 1.65%. This region is one of the main corn production areas of China. In 2012, the dominant vegetation in the flux matrix area consisted of corn (67%), vegetables (7%), orchard species (3%), and shelter forest (3%). The other major land cover types are residential areas (10%) and roads (9%).

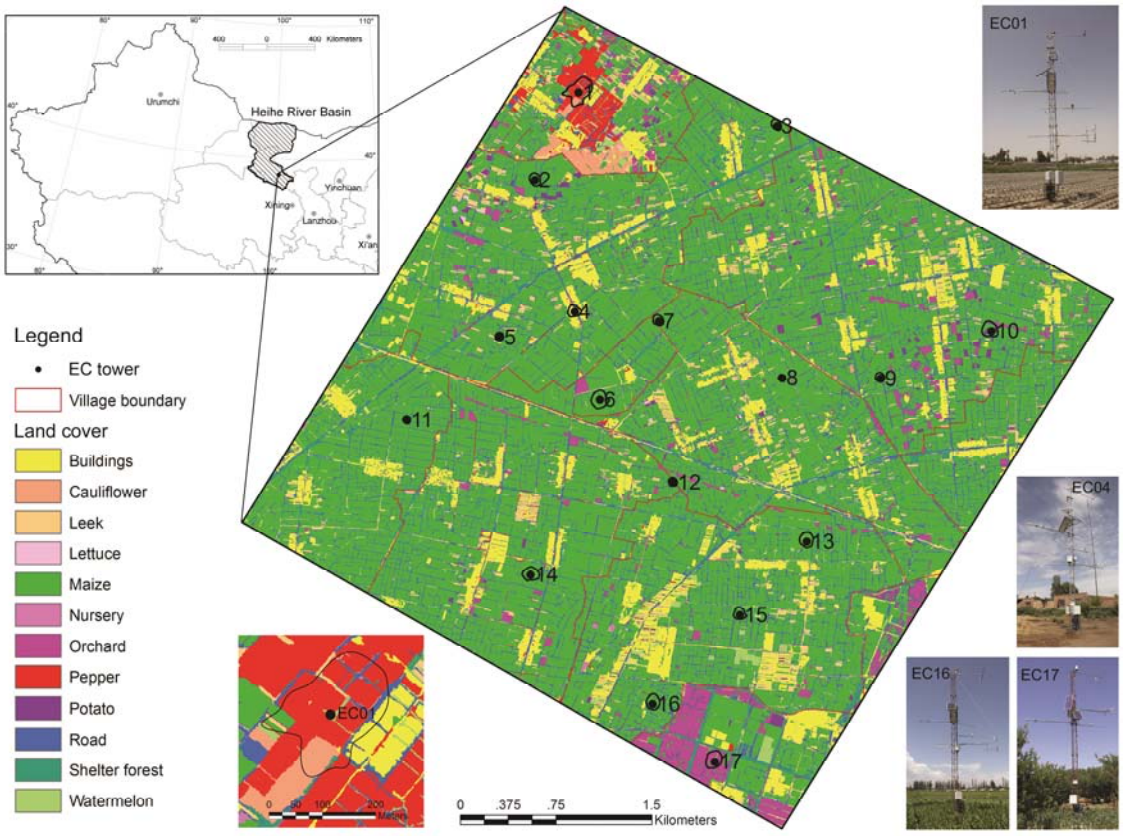

Figure 1. Map of the study area showing the set up of the EC towers. (The land cover map was derived from hyperspectral imagery combined with LiDAR data from an airborne survey conducted in 2012. The black lines around the EC towers denote the daily aggregated 80% footprint contours for July 19, 2012).

2.2 HiWATER-MUSOEXE

HiWATER was designed as a comprehensive ecohydrological experiment implemented in the Heihe River Basin -- an inland river watershed (Li et al., 2013; Xu et al., 2013). As a component of HiWATER, MUSOEXE was implemented to reveal the spatial heterogeneities of carbon and water flux by constructing a flux matrix from May to September 2012. The matrix includes 17 EC systems together with automatic weather stations that were installed in the core experimental area (5 km × 5 km) according to the underlying surface characteristics, i.e., the distribution of crop type, windbreak forest, residential area, soil moisture, and irrigation status. In this way, the maximum heterogeneity in carbon flux over the entire experimental area (5 km × 5 km) can be captured. Airborne VNIR (visible and near infrared) imaging spectrometers, i.e., the Compact Airborne Spectrographic Imager (CASI) and the Shortwave Infrared Airborne Spectrographic Imager (SASI), were used to measure the leaf area index (LAI), fraction of PAR (FPAR), fraction of vegetation cover (FVC), and land surface temperature (LST). Airborne LiDAR and CCD cameras were used to measure the vegetation structure and to estimate the aerodynamic roughness. Approximately 180 wireless soil moisture sensors were used to capture the spatiotemporal variations in soil moisture across the heterogeneous land surface (Jin et al., 2014). A more detailed description of HiWATER-MUSOEXE can be found in Liu et al. (2016).

2.3 EC measurements and data processing

In this study, EC data from 17 towers within the 5 km × 5 km area were used. The details of these EC systems are shown in Table 1. The sensor height was selected depending on the underlying land cover type. Daily NEP (-NEE) values were derived from 10 June to 14 September 2012.

The consistency of all EC systems and data quality were ensured by the following steps. First, the consistency of the EC instruments was tested during an inter-comparison campaign in the flat, open Gobi desert, over a surface covered by coarse grain sand and small pebbles with withered sparse scrub vegetation. This campaign was completed before HiWATER-MUSOEXE was conducted (Xu et al., 2013). Second, all raw data were acquired at 10 Hz and processed using the EdiRe software package (http://www.geos.ed.ac.uk/homes/rclement/micromet/EdiRe/). The processing included spike removal (Højstrup, 1993), lag time correction (McMillen, 1988), coordinate rotation (Wilczak et al., 2001), frequency response correction (Moore, 1986), sonic virtual temperature correction (Schotanus et al., 1983), a non-steady state test, an integral turbulence test (Foken and Wichura, 1996), WPL correction (Webb et al., 1980), and averaging to half-hourly fluxes. Third, quality control of the half-hourly flux data output from EdiRe was carried out as suggested by Liu et al. (2011) and Blanken et al. (1998). Fourth, empirical gap filling was applied. The missing daytime data were gap-filled using the 'look-up' table method (Falge et al., 2001), which is based on empirical relationships between NEE, air temperature and incident PAR determined for each site. The missing nighttime data were estimated using the van't Hoff equation (Zhang et al., 2015). Finally, the gap-filled half-hourly NEE data were aggregated to daily values using a sum function.

Ecosystem respiration (Re) was obtained by summing nighttime NEE and daytime estimates of Re. The latter was estimated based on the nighttime NEE-temperature relationship derived using the van't Hoff equation (Lloyd and Taylor, 1994). The daily GPP was calculated as NEP+Re. GPP and Re were used to determine the dominant factor affecting the observed variability of NEP.

Table 1. The eddy covariance system matrix of HiWATER- MUSOEXE.

No.	Latitude (°N)	Longitude (°E)	Elevation (m)	Sensor height (m)	Dominant underlying surface type
EC01	38.89322	100.35813	1552.75	3.8	Vegetables
EC02	38.88695	100.35406	1559.09	3.7	Corn
EC03	38.89053	100.37634	1543.05	3.8	Corn
EC04	38.87752	100.35753	1561.87	4.2, 6.2 after 19 Aug.	Residential area
EC05	38.87574	100.35068	1567.65	3	Corn
EC06	38.87116	100.35970	1562.97	4.6	Corn
EC07	38.87676	100.36521	1556.39	3.8	Corn
EC08	38.87254	100.37649	1550.06	3.2	Corn
EC09	38.87239	100.38546	1543.34	3.9	Corn
EC10	38.87567	100.39572	1534.73	4.8	Corn
EC11	38.86991	100.34197	1575.65	3.5	Corn
EC12	38.86515	100.36631	1559.25	3.5	Corn
EC13	38.86074	100.37852	1550.73	5	Corn
EC14	38.85867	100.35310	1570.23	4.6	Corn
EC15	38.85551	100.37223	1556.06	4.5	Corn
EC16	38.84931	100.36411	1564.31	4.9	Corn
EC17	38.84510	100.36972	1559.63	7	Orchard

2.4 Mapping land cover type

Assessing the influence of heterogeneous vegetation structure on EC fluxes and the representativeness of EC towers requires high spatial and thermal resolution information of the land cover type. In this study, a land cover type map with a 1-m spatial resolution was used. The map was derived from airborne hyperspectral imagery (CASI system) and the Canopy Height Model (CHM) data from airborne LiDAR acquired during the growing season using an object-based classification method. The accuracy of the land cover type map is higher than 90%. More details on the map can be found in Liu and Bo (2015).

2.5 Acquisition of satellite remote sensing data

Remotely sensed data at high spatial and temporal resolution are needed for upscaling EC-based NEP measurements to the grid scale. However, it is difficult to acquire appropriate remotely sensed data with both high spatial and temporal resolution due to current technical limitations. Landsat imagery with a 30-m spatial resolution is well suited for characterizing landscape-level vegetation structure, but offers only a 16-day revisit cycle that is often increased by cloud contamination. In contrast, MODIS has a higher temporal resolution, but a coarser spatial resolution. In this study, high temporal resolution Landsat-like data were used, which were produced by blending Landsat and MODIS data using algorithms as suggested by Zhu et al. (2010).

Five cloud-free scenes of Landsat 7 ETM+ images (20120624, 20120710, 20120811, 20120827, and 20120912) and fifteen eight-day MODIS Terra reflectance products (MOD09A1) with a spatial resolution of 500 m over the period from 1 June to 21 September 2012 were obtained from the USGS (US Geological Survey) GLOVIS portal (http://glovis.usgs.gov/). Gaps in the five acquired scenes of the Landsat 7 ETM+ SLC-off data were filled using a Neighborhood Similar Pixel Interpolator (NSPI) proposed by Chen et al. (2011). Then, the Landsat images were georeferenced and atmospherically corrected using the Fast Line-of-sight Atmospheric Analysis of Spectral Hyper cubes (FLAASH) model implemented in the ENVI software. The MODIS data were reprojected to the Universal Transverse Mercator (UTM) projection using the MODIS reprojection tool, resampled to a 30-m spatial resolution using a nearest neighbor approach, and clipped to the extent of the available Landsat images. Finally, the Landsat-like data with an 8-day interval were produced by blending the Landsat and MODIS data using the Enhanced Spatial and Temporal Adaptive Reflectance Fusion Model (ESTARFM) of Zhu et al. (2010).

3 Methodology

The overall framework for evaluating the spatial representativeness of the EC carbon flux measurements and the uncertainty associated with upscaling NEP from the tower scale to the grid scale includes four aspects (Figure 2). First, the spatial representativeness of the single tower EC flux measurements relative to the source area of the 17 EC towers was evaluated by conducting temporal stability analysis. This approach was first proposed by Vachaud et al. (1985) and later successfully used to evaluate the temporal stability of soil moisture (Schneider et al., 2008). The approach assumes that the mean grid soil moisture can be represented by single measurements selected from a larger measurement volume (Schneider et al., 2008). Recently, this method was used to analyze the temporal and spatial patterns of carbon dioxide fluxes (Kreba et al., 2013). The second aspect was to determine the influence of landscape structure on the representativeness of the EC towers by analyzing the relationship of the EC representativeness and the high-resolution land cover type fraction within the footprint area. Then, some indicators were proposed based on the relationship of the land cover type fraction between the footprint area of the EC towers and the grid, and were used to improve the representativeness of the EC flux measurements. We assumed that in an agricultural landscape, environmental factors are dominated by land cover type because factors such as temperature, soil moisture, and even atmospheric turbulence characteristics are highly correlated with land cover structure in a cropland landscape (Baldocchi and Ma, 2013). Finally, the original EC flux data and representativeness-corrected EC flux data at the 17 sites were upscaled to the grid scale using the model-data fusion method. The mean of 17 grid-scale NEP estimates based on corrected EC flux data was defined as a reference to examine the uncertainty of the representativeness error associated with the estimation of NEP at the grid scale and to determine the ability of the proposed indicators to reduce the representativeness error. Details on this approach are provided in the following sections.

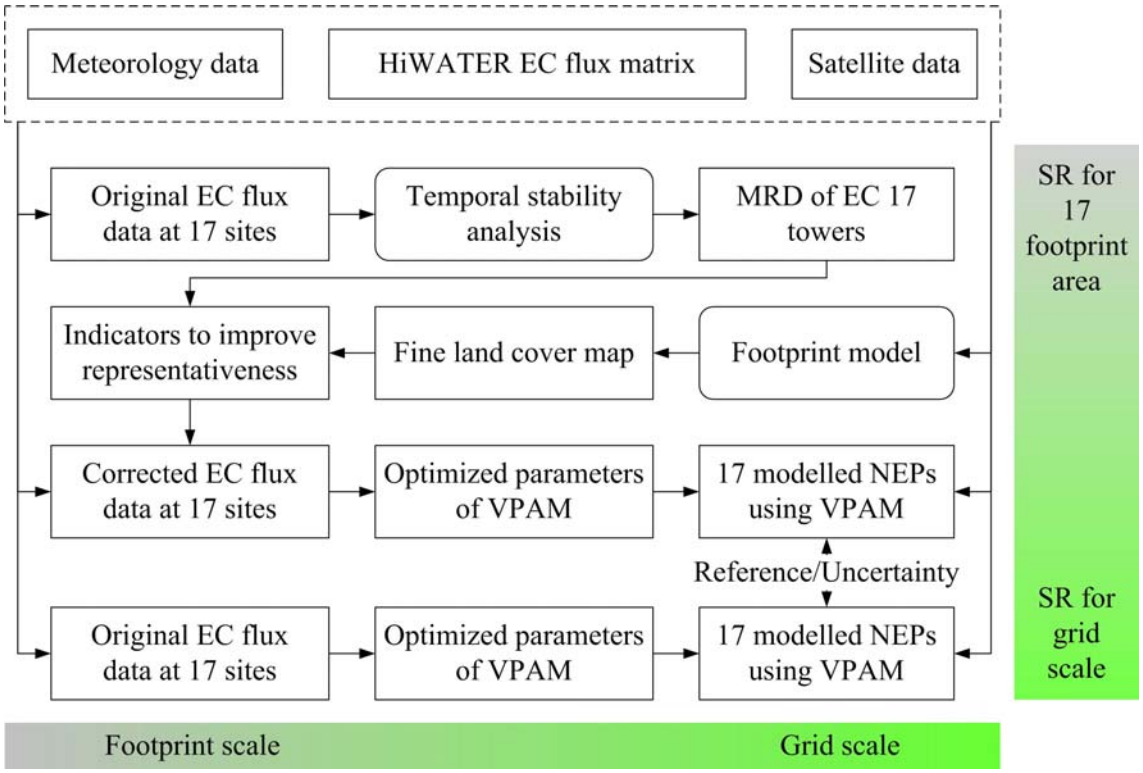

Figure 2. Framework of the evaluation of spatial representativeness (SR) and uncertainty of EC NEP measurement for upscaling to the grid scale.

3.1 Evaluation of the representativeness of the EC flux observations

For the temporal stability method, the representativeness of the CO_2 fluxes measured by each EC tower was determined by the mean relative difference (MRD) and standard deviation of the MRD (SDMRD). The MRD is defined as

$$\overline{\delta}_i = \frac{1}{t}\sum_{j=1}^{t}\frac{S_{i,j} - \overline{S}_j}{\overline{S}_j} \quad (1)$$

where $S_{i,j}$ is the jth sample at the ith tower of n EC sites within the grid (n=17 in this study), and $\overline{S}_j$ is the mean carbon flux calculated across all towers over a given time j (j =1 to t). The SDMRD is calculated as follows:

$$\sigma(\delta_i) = \sqrt{\frac{1}{t-1}\sum_{j=1}^{t}\left(\frac{S_{i,j} - \overline{S}_j}{\overline{S}_j} - \overline{\delta}_i\right)^2} \quad (2)$$

The MRD quantifies the systematic bias of the CO_2 fluxes at each tower location with respect to the grid mean of the 17 EC footprints. Any EC tower with an MRD close to zero is considered to have a small systematic bias to represent NEP at the grid scale. In practice, once an EC tower is installed at a designated location, it is not easily moved. The ability of a particular tower to unbiasedly capture the mean flux at the grid scale over a long-term period is very important. The SDMRD characterizes the precision of the bias. A small SDMRD indicates low variance of the representativeness. If a tower has both small MRD and SDMRD, it can be concluded that it accurately and precisely represents the mean grid-scale carbon flux over long time periods. Consequently, Jacobs et al. (2004)

proposed a root mean square error (RMSE) that quantifies the representativeness of a specific location by combining the MRD and SDMRD as follows:

$$RMSE_i = \sqrt{\bar{\delta}_i^{\,2} + \sigma(\delta_i)^2} \quad (3)$$

3.2 Footprint modeling

The contribution of each land cover type to the measured flux was assessed using the footprint parameterization method of Kljun et al. (2015), which is an updated version of the previous parameterization developed by Kljun et al. (2004). This parameterization is based on the backward Lagrangian stochastic footprint model LPDM-B (Kljun et al., 2002) and is one of a limited number of footprint approaches that is applicable within or above the surface layer; consequently, this parameterization can be used for convective, neutral and stable stratification of the boundary layer.

The footprint parameterization was run on turbulence data (half-hourly temporal resolution) from each of the EC towers at the study site. The roughness lengths and zero-plane displacement heights were interpolated from weekly measurements of the canopy height at all study sites using the ratios suggested by Grimmond and Oke (1999) and Kaimal and Finnigan (1994). The half-hourly footprint estimates were combined with land cover type determined from the LiDAR/optical data fusion classification, and the footprint-weighted land cover contributions were summed and normalized over 24-hour periods. Subsequently, the 80% daily footprint contours were used.

3.3 VPRM Model

VPRM is a satellite data-based light use efficiency model that uses remotely sensed indices and meteorological variables to estimate NEP (Mahadevan et al., 2008). VPRM is based on the Vegetation Photosynthesis Model (VPM) of Xiao et al. (2004a, 2004b), combined with ecosystem respiration (R) to provide NEP estimates. In VPRM, NEP is derived as

$$NEP = \lambda \times T_{scale} \times P_{scale} \times W_{scale} \times \frac{1}{(1 + PAR / PAR_0)} \times EVI \times PAR - \alpha \times T - \beta \quad (4)$$

where, λ, PAR_0, α, and β are the four model parameters, namely, the product of the maximum quantum yield, the radiation scale factor, the temperature sensitivity factor, and the model offset, respectively. These parameters were derived from the flux tower data. Photosynthetically active radiation (PAR) and air temperature (T) were measured at all flux tower sites. The Enhanced Vegetation Index (EVI) was derived from synthetic Landsat ETM+ images as suggested by Huete et al. (1997).

T_{scale}, P_{scale}, and W_{scale} represent the temperature sensitivity of photosynthesis, the effects of leaf age on canopy photosynthesis, and the effect of water stress on NEE, respectively. T_{scale} was calculated using the equation developed for the Terrestrial Ecosystem Model (Raich et al., 1991):

$$T_{scale} = \frac{(T - T_{\min})(T - T_{\max})}{(T - T_{\min})(T - T_{\max}) - (T - T_{opt})^2} \quad (5)$$

where *Tmin*, *Tmax*, and *Topt* are minimum, maximum, and optimal temperatures (℃), respectively, for photosynthesis. *Topt* was set to 20℃.

For P_{scale}, LSWI (Land Surface Water Index) was used to identify phenology (Boles et al., 2004; Xiao et al., 2004a). During the period from bud burst to full leaf expansion, i.e., 10 May to 25

August at the study site, P_{scale} was calculated as

$$P_{scale} = \frac{1 + LSWI}{2} \quad (6)$$

After full leaf expansion, P_{scale} was set to 1.

W_{scale} can be expressed as

$$W_{scale} = \frac{1 + LSWI}{1 + LSWI_{\max}} \quad (7)$$

where $LSWI_{\max}$ is the maximum LSWI within the plant growing season for each site (or pixel).

3.4 Estimating the VPRM parameters

Following Chen et al. (2010), we estimated the VPRM model parameters (cf. Section 3.3) by minimizing the differences between the modeled and EC-measured NEP, i.e., by minimizing the cost function:

$$J(p) = \frac{1}{2}\left[(Y_o - Y(p))^T C_o^{-1}(Y_o - Y(p)) + (p - p_b)^T P_b^{-1}(p - p_b)\right] \quad (8)$$

where Y_o represents the data vector, $Y(p)$ is the model output vector, and C_o and P_b are the error covariance matrices of the data and model parameters, respectively. p is the parameter vector and p_b represents the a priori values of p. The input data, such as T_{scale}, P_{scale}, W_{scale}, and EVI, were integrated from blended-Landsat pixels to the footprint area using the mean values because the Landsat resolution (30-m) does not match the EC scale. We adopted a gradient-based algorithm (Levenberg-Marquardt algorithm) to solve Equation (8). The four VPRM parameters were optimized using the data from the 17 EC flux towers. Then, the 17 site-specific parameter groups were used to estimate the regionally gridded NEP for the study site. Finally, for each parameter group, the mean modeled NEP within the 5 km × 5 km area was compared with the arithmetic mean NEP measured at the 17 EC towers.

The representativeness error of each EC site was evaluated using the Pearson correlation coefficient (R), the mean difference (MD), and the standard deviation of the MD (SDMD).

3.5 Improving the representativeness of the EC NEP measurement

To improve the representativeness of the EC measurements, an indicator as a proxy for the MRD of the EC towers is needed. In this study, we used four indices to improve the representativeness of the EC measurements based on the difference in the mean EVI (DMEVI) and fraction of land cover type (LCfrac) between each EC footprint area and the total footprint area for all 17 EC towers. These indices include the DMEVI, the LCfrac, the estimated MRD based on the DMEVI (MRD'_E), and the estimated MRD based on the LCfrac (MRD'_F). The LCfrac was calculated by combining the negative and positive effects of different land cover types using Equations (9) to (11). For positive NEP land cover types, i.e., vegetation, such as corn and trees, Equation (9) was used, whereas Equation (10) was used for negative or zero NEP land cover types, such as roads and buildings. The contribution to NEP varies among the different land cover types. In practice, if prior knowledge of

this contribution is available, it should be used as a weighting factor to estimate this index. In general, a land cover type with a larger absolute NEP should be assigned a higher weight. The equations used are as follows:

$$\mathrm{LCfrac}_p = \sum_{type=1}^{n} W_{type} \times (F_{type,ec} - F_{field}) \quad (9)$$

$$\mathrm{LCfrac}_n = \sum_{type=1}^{n} W_{type} \times (F_{field} - F_{type,ec}) \quad (10)$$

$$\sum_{type=1}^{n} W_{type} = 1 \quad (11)$$

$$\mathrm{LCfrac} = \mathrm{LCfrac}_p + \mathrm{LCfrac}_n \quad (12)$$

where F is the fraction of land cover type for the study site or the footprint area of an EC tower, and W is the weighting factor of each land cover type. The W of each land cover type, i.e., 0.3 (corn), 0.06 (orchard, trees), 0.01 (leek, lettuce, cauliflower, nursery, potato, watermelon), 0.02 (pepper), and 0.25 (buildings, roads), used in this study was determined by expert knowledge. The result is only sensitive to the order of absolute NEP and is not sensitive to the exact weight for a specific land cover type.

4 Results and discussion

4.1 Spatial variability of NEP, Re, and GPP

Knowledge of the spatial and temporal variability of NEP, Re, and GPP during a study period is essential for understanding the representativeness of EC measurements at the grid scale. The arithmetic mean and standard deviation of NEP, Re, and GPP calculated from the 17 EC towers at the study site are shown in Figure 3.

Large variability in GPP, Re, and NEP (error bars in Figure 3) was found among the 17 EC towers during the growing season from 10 June to 14 September 2012. The variability increased with an increase in GPP and NEP. This result was expected as the difference between vegetated and non-vegetated fluxes increases with vegetation growth. The within-site variability was almost constant after the corn canopies reached a ceiling (DOY: 190), followed by a decrease after the crop harvest (DOY: 240). The fluctuations may have been caused by disturbance from the de-tasseling process of the seed corn from DOY 220 to 230. The large variability found within the study site, i.e., kilometer-sized pixels that are usually expressed as a single cropland type at the global scale, indicates the significant impact of sub-pixel-scale crop type on the grid-mean GPP and NEP.

Precipitation and irrigation are key factors for photosynthesis, and hence crop growth was sustained during the growing season from June to September. However, GPP, Re, and NEP were reduced during precipitation events due to limited concurrent incoming radiation and low temperature (Figure 3). Within the study area, more than 5000 individual fields were irrigated daily on an individual basis according to the crop water requirements and the water-usage agreements among approximately 6 village groups and 51 villages. The impact of irrigation variability on the process feedbacks associated with GPP, Re, and NEP is complex (Borken and Matzner, 2009; Jabro et al., 2008), but enhanced photosynthesis and increased net CO_2 uptake were generally observed during the first half of the growing season.

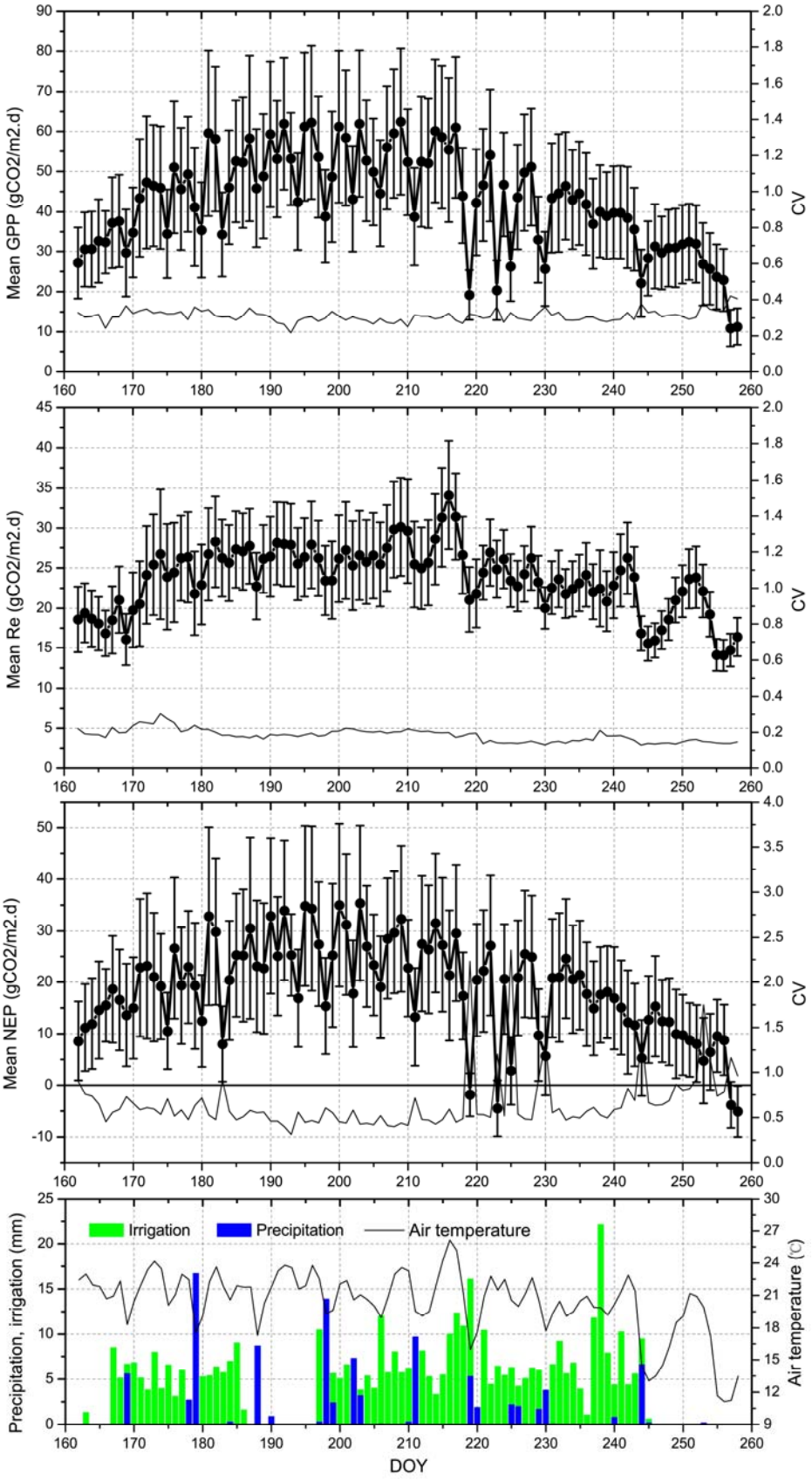

Figure 3. Study site mean (dot) and standard deviation (error bar) of GPP, Re, and NEP during the study period in 2012, and irrigation, precipitation, and air temperature over the same time period.

4.2 Representativeness of EC tower measurements

The large variability of GPP, Re, and NEP within the study site raises the question of whether some EC towers are more representative than others with respect to the footprint area NEP of all EC towers. The answer is yes. The MRD, SDMRD, and RMSE for GPP, Re, and NEP are presented in Figure 4. EC towers with MRDs greater than zero would systematically overestimate the mean area value, and those below zero would underestimate it. These systematic underestimations reached 92(±11)%, 30(±11)%, and 165(±150)% in extreme cases for GPP, Re, and NEP, respectively. The overestimations reached 25(±14)%, 20(±13)%, and 40(±33)% for GPP, Re, and NEP, respectively. EC04, EC01, and EC17 were the least representative for both GPP and NEP as the dominating underlying surface type within their footprint area was residential, vegetables, and orchards, respectively, which differed from the dominant underlying surface type (corn) of the study area. However, EC01 and EC17 were representative for Re as their Re was comparable to corn sites. This was expected as Re had a lower spatial variability than GPP and NEP, as shown in Section 4.1. Variability in Re existed mainly between vegetation and non-vegetation sources, in contrast to GPP and NEP, for which variability existed among different vegetation types, including vegetable plots, orchards and corn. For example, even for EC towers that appeared to have the same crop type within the footprint area (all towers except EC04, EC01, and EC17 were associated with the same dominant underlying surface type, i.e., corn), the representativeness error of the EC towers was significantly large. The representativeness error resulting from small-scale variability of GPP and NEP illustrates the necessity to improve the understanding of the representativeness of EC towers and the potential usefulness of high resolution (spatial and temporal resolution) land cover type information.

The most representative towers (smallest RMSE) for GPP, Re, and NEP at the study site were EC09, EC10, and EC05, respectively (Figure 4, Table 2). Relative to the mean value calculated from the 17 towers, the representativeness error (MD) of EC09, EC10, and EC05 for GPP, Re, and NEP was 1.74(±2.55), 0.98(±2.09), and 1.25(±2.48) g CO_2 m^{-2} d^{-1}, respectively (Table 2). Although the representativeness differed for GPP, Re, and NEP, the correlation coefficient of the RMSE index of NEP and GPP or Re was significant, i.e., 0.95 and 0.75, respectively. This shows that the dynamics of NEP were more strongly correlated with the dynamics of GPP than with Re. These findings further illustrate that NEP was dominated by rapid increases in GPP in the study area.

Therefore, although EC is considered as the most direct NEP observation tool at the ecosystem scale, for heterogeneous land cover types it may be problematic to validate remotely sensed NEP products at the global scale by direct comparison. This results from the different fractions of land cover types within the EC footprint and the respective grid. Clarification of the relationship of the fraction of land cover type between the EC footprint area and the study site is useful not only for the selection of the optimal EC location but also for upscaling EC-based NEP to a pixel scale to validate remotely sensed NEP products.

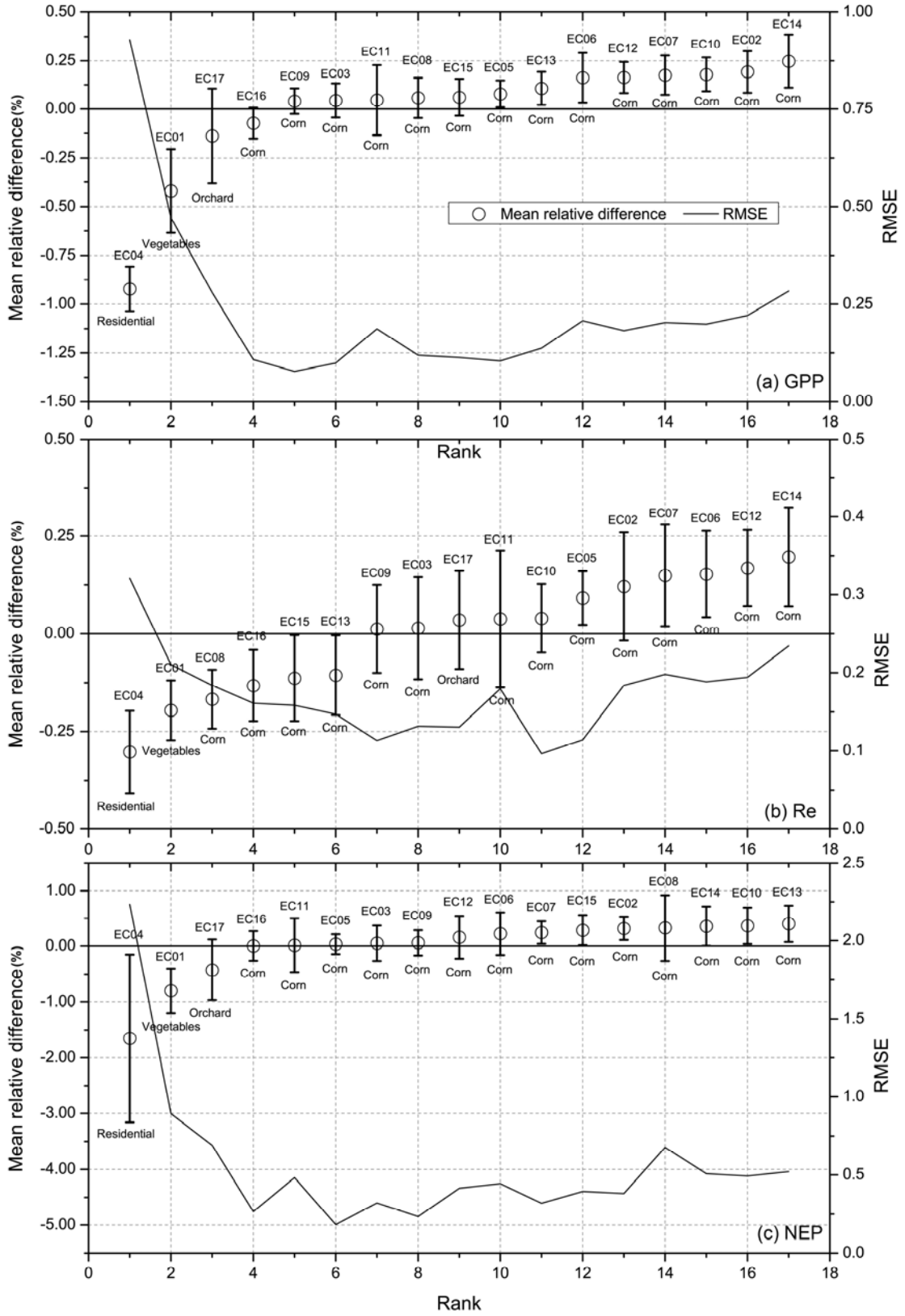

Figure 4. The mean relative difference (MRD, open circles), standard deviation of the MRD (SDMRD, error bars) and RMSE (solid lines) of individual EC tower measurements (EC01 to EC17, Table 1) for (a) GPP, (b) Re, (c) NEP, ordered by rank.

Table 2. Assessment of representativeness of each EC tower for grid-mean GPP, Re, and NEP.

	GPP				Re				NEP			
No.	**R**	**RMSE**	**MD**	**SDMD**	**R**	**RMSE**	**MD**	**SDMD**	**R**	**RMSE**	**MD**	**SDMD**
EC1	0.60	21.25	-18.79	9.98	0.84	5.25	-4.75	2.23	0.44	16.61	-14.04	8.92
EC2	0.98	9.70	8.58	4.55	0.89	4.70	3.10	3.55	0.96	6.42	5.48	3.36
EC3	0.97	3.68	1.80	3.23	0.82	3.19	0.44	3.18	0.96	2.98	1.36	2.67
EC4	0.38	40.54	-38.94	11.34	0.73	8.32	-7.59	3.43	0.32	32.57	-31.35	8.89
EC5	0.98	4.71	3.51	3.16	0.95	2.82	2.26	1.70	0.98	2.76	1.25	2.48
EC6	0.94	8.34	6.66	5.05	0.84	4.11	3.40	2.31	0.92	5.77	3.26	4.79
EC7	0.96	8.78	7.58	4.46	0.84	4.66	3.53	3.05	0.97	5.31	4.05	3.46
EC8	0.98	5.19	3.14	4.15	0.93	4.19	-3.86	1.64	0.96	7.99	7.01	3.86
EC9	0.98	3.08	1.74	2.55	0.81	2.75	0.23	2.75	0.96	3.51	1.50	3.19
EC10	0.97	8.47	7.50	3.95	0.91	2.30	0.98	2.09	0.94	7.80	6.52	4.30
EC11	0.93	7.50	2.99	6.92	0.72	4.64	1.00	4.55	0.94	6.28	1.99	5.99
EC12	0.98	7.49	6.77	3.22	0.93	4.75	4.10	2.42	0.95	4.09	2.67	3.12
EC13	0.98	6.16	4.82	3.86	0.90	3.30	-2.35	2.33	0.97	7.87	7.16	3.27
EC14	0.95	11.43	10.23	5.14	0.89	5.79	4.80	3.25	0.93	6.74	5.43	4.01
EC15	0.96	4.54	2.51	3.81	0.77	3.90	-2.78	2.76	0.97	6.04	5.29	2.93
EC16	0.97	4.28	-2.67	3.36	0.85	3.89	-3.14	2.30	0.97	2.91	0.47	2.89
EC17	0.77	10.78	-7.40	7.88	0.78	2.74	0.64	2.68	0.67	10.54	-8.04	6.86

Note: four statistical indices were used to evaluate the representativeness of each EC site: the Pearson correlation coefficient (R), root mean square error (RMSE), the mean difference (MD), and the standard deviation of the MD (SDMD). See text for more details. The units of the last three indices are g CO_2 m^{-2} d^{-1}.

4.3 Characteristics of tower representativeness and the correction of representativeness

The relationship between the tower characteristics and representativeness is presented in Figure 5. This relationship shows that high representativeness is indicated by small differences in the fraction of land cover type or mean EVI between the footprint of an individual EC tower and the footprint of all EC towers. As shown in Figure 5a, both the DMEVI and LCfrac correlated well with the MRD, with correlation coefficients of 0.95 and 0.93, and RMSEs of 0.03 and 0.04, respectively. Based on these correlations, the DMEVI and LCfrac can be used as direct proxies for the MRD or to estimate the MRD'_E and MRD'_F using Equations (13) and (14), although further validation of the relationship between the MRD and the DMEVI and LCfrac is needed. With respect to the four indices presented above, a negative index indicates that the EC measurement systematically underestimates the grid-mean NEP, and a positive index points to overestimation. This information can be used to correct the representativeness of the original EC NEP measurements using Equation (15).

$$MRD'_E = 5.85 \times DMEVI \quad (13)$$

$$MRD'_F = 4.38 \times LCfrac \quad (14)$$

$$NEP_{ec\_correct} = \begin{cases} \left|MRD' \times NEP_{EC}\right| + NEP_{EC} & \text{if MRD' is negative} \\ -\left|MRD' \times NEP_{EC}\right| + NEP_{EC} & \text{if MRD' is positive} \end{cases} \quad (15)$$

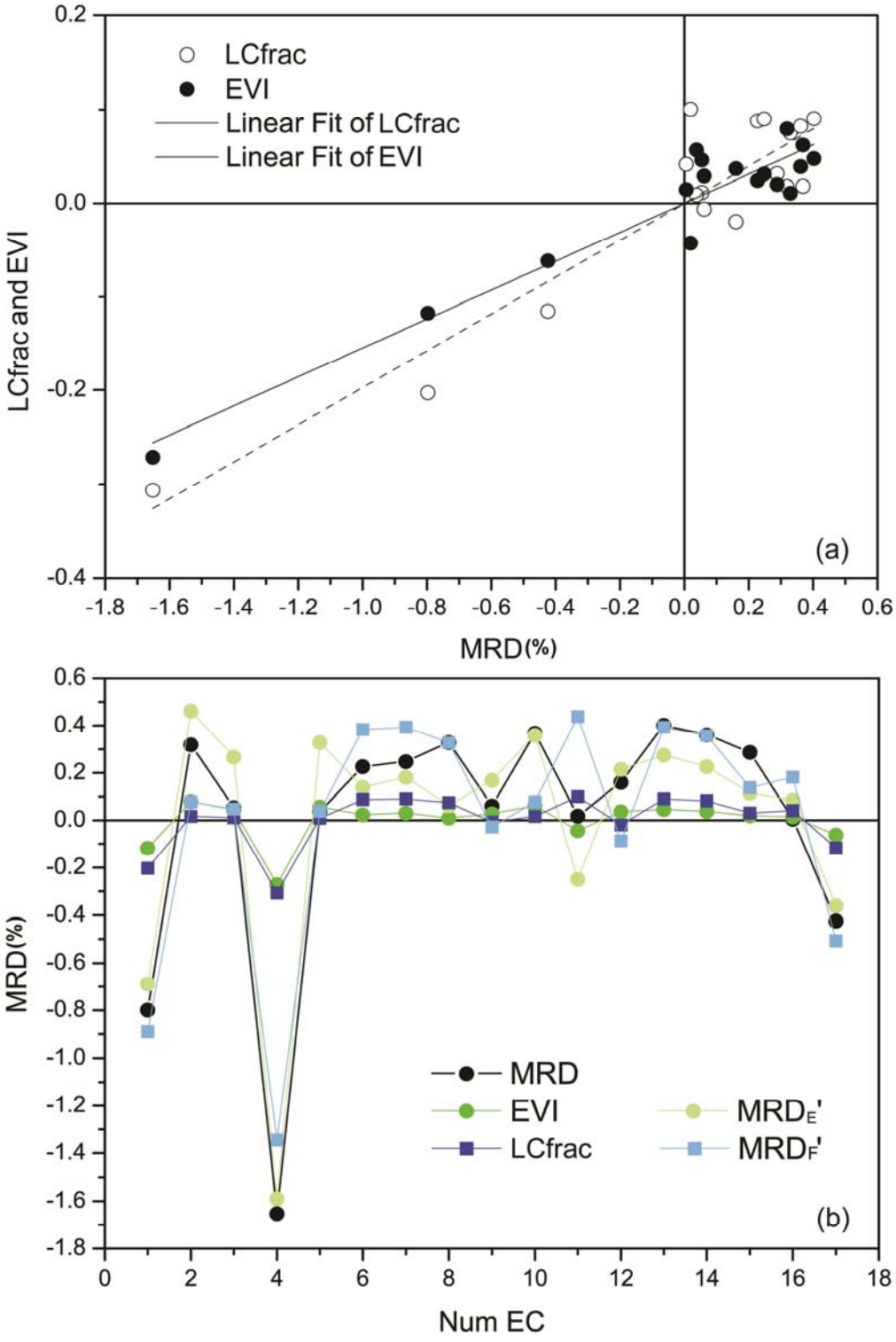

Figure 5. Consistency of the four proxy indicators (i.e., DMEVI, LCfrac, $MRD_E^{'}$, and $MRD_F^{'}$) with mean relative difference (MRD).

The variabilities of the above four indices with the EC MRD are shown in Figure 5b. The MD of the LCfrac with an MRD was 0.28(±0.31) and slightly smaller than the MD of 0.29(±0.33) for the DMEVI. This indicates that the effect of using the LCfrac and DMEVI is similar, and the former may be more effective for some landscapes, such as the artificial landscape of the study site. GPP and Re are impacted by the spatial distribution of soil moisture (irrigation), soil temperature, and other crop field management practices that are implemented according to crop type. However, the MD of MRD'_F with an MRD was 0.14(±0.13) and slightly larger than the MD of 0.13(±0.08) for MRD'_E. Hence, at some EC sites, over-correction of the MRD occurred, and this was more pronounced for MRD'_F than for MRD'_E. As observed in Figure 5b, this over-correction for the EC03, EC05, and EC11 sites was more pronounced for MRD'_F than for MRD'_E, but the LCfrac was closer to the MRD than the DMEVI. This will be further discussed in the next section. This over-correction may be due to uncertainties in measurements, data processing, and its inherent inconsistency. For example, for EC05 and EC08, the sensor was within the roughness sublayer during the growing season, and hence there was considerable uncertainty associated with the flux measurements, and the footprint model was applied outside its limits. Additional factors, such as the heterogeneity of soil temperature and soil moisture within a land cover type, may also cause inconsistency. Further, the coefficient of the simple relationship was only verified at this study site; it may be related to heterogeneity at a sub-grid scale and this needs to be verified in other heterogeneous landscapes.

4.4 Impact of the representativeness of EC measurements with respect to estimating grid-scale NEP

Upscaling the EC NEP measurements from the 17 towers using a model-data fusion method resulted in 17 estimates of grid-scale NEP. As depicted in Figure 6a, the 17 estimates of grid NEP showed large variability with a mean SD of 7.61(±1) g $CO_2\,m^{-2}\,d^{-1}$, although in most cases, the variability was smaller than the variability of the original EC NEP measurements from the 17 sites, with a mean SD of 10.2(±2.86) g $CO_2\,m^{-2}\,d^{-1}$. The mean MD between the mean modeled grid NEPs and mean NEPs of the 17 EC measurements was significant, i.e., 5.65(±2.97) g $CO_2\,m^{-2}\,d^{-1}$. For the EC05 tower, the mean MD of the NEP between the measured and modeled value was 6.83(±3.56) g $CO_2\,m^{-2}\,d^{-1}$. This difference further highlights that even 17 towers within a 5 km × 5 km study area do not necessarily represent the true NEP at the grid scale. The EC measurements need to be upscaled before remotely sensed NEP products or NEP estimated using ecosystem models are validated against them. These findings also show that parameters of VPRM depend on the scale and spatial heterogeneity. The parameters of VPRM estimated using the 17 EC towers at a similar landscape scale exhibited significant spatial variability due to differences in the fraction of land cover type within the tower footprints. The essence of scale dependence of the VPRM parameters is associated with the variability of the parameters. Therefore, the key component of the upscaling process is to obtain representative parameters that are naturally related to the spatial heterogeneity of the target grid, i.e., the representativeness of the EC measurement with respect to the grid scale. This also highlights that the mean parameter groups are specific to each land cover type. This is common practice in current land surface models or remote sensing-based models. The parameter are determined at a sub-pixel scale based on limited EC measurements, which are then interpolated to the pixel scale according to a coarse land cover map and may result in significant bias in NEP estimation at a regional scale because the heterogeneity of land cover type is ignored at the sub-grid scale. The uncertainty of scale mismatch between remote sensing-based NEP products and reference data may result in a greater uncertainty when validating results.

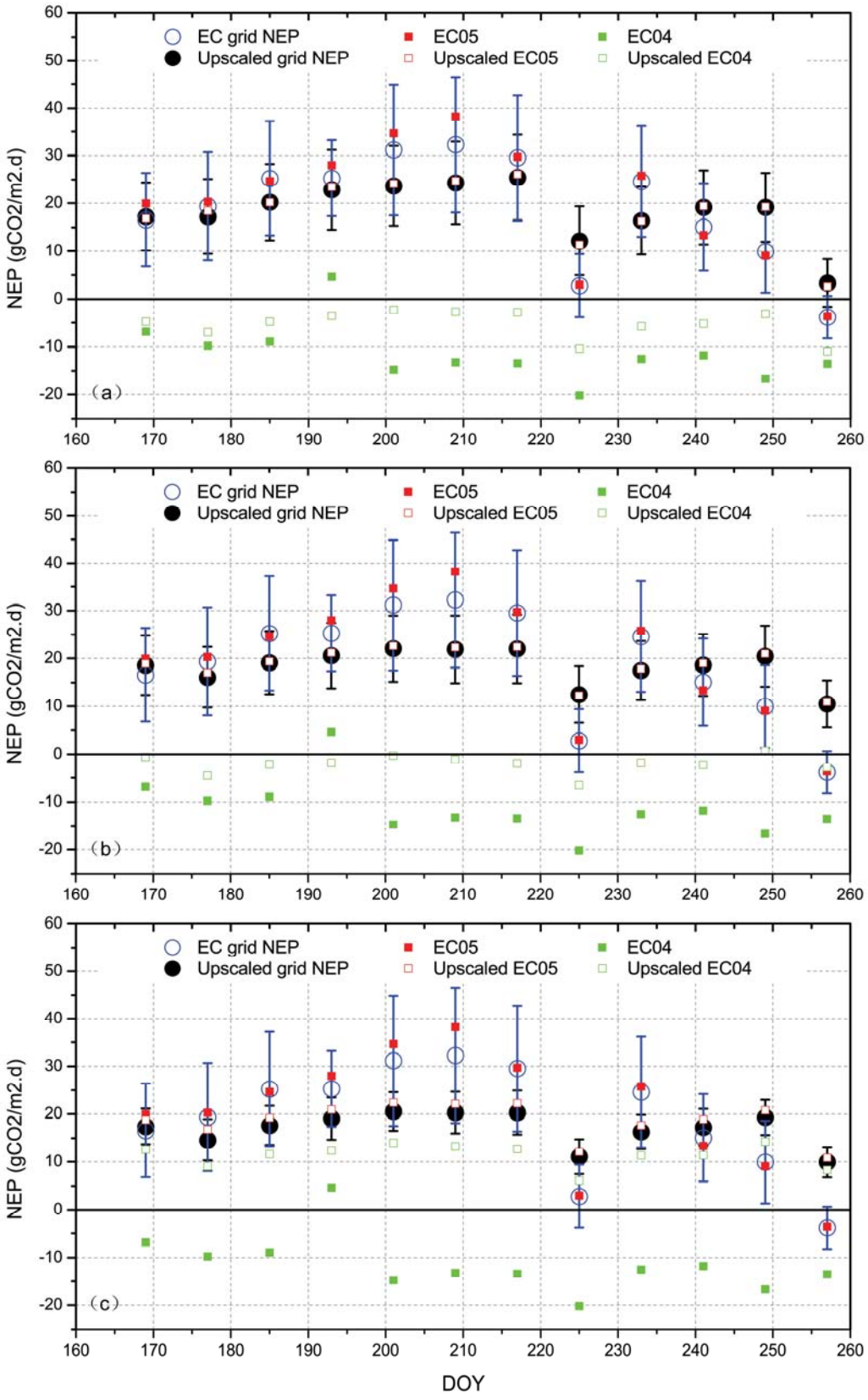

Figure 6. Impact of representativeness of EC measurements for upscaling NEP to the grid scale (a) Upscaled using original EC data; (b) Upscaled using corrected EC data using LCfrac; (c) Upscaled using corrected EC data using MRD_F).

Most of the 17 grid-scale NEP values modeled using the model-data fusion method were improved by correcting the representativeness of the corresponding EC measurements from the 17 sites using the LCfrac, DMEVI, MRD'_F, and MRD'_E proxies calculated for the footprint of each tower relative to the grid area (5 km × 5 km area). Here, we focus on LCfrac and MRD'_F, as DMEVI and MRD'_E showed similar behavior. The modeled grid-scale NEPs based on the model-data fusion method and the corrected EC measurements using LCfrac and MRD'_F are shown in Figure 6b and Figure 6c, respectively. Compared with the modeled NEPs using the original EC measurements (Figure 6a), the variability of the modeled mean grid NEPs based on the corrected EC measurements decreased. The mean SD of the modeled NEPs at the grid scale decreased from 7.61(±1) g CO_2 m^{-2} d^{-1} (no correction) to 6.41(±0.58) g CO_2 m^{-2} d^{-1} (LCfrac) and 3.96(±0.4) g CO_2 m^{-2} d^{-1} (MRD'_F). The mean MD between each modeled NEP using the corrected EC measurements from the 17 towers and the modeled mean grid NEP using the 17 corrected EC measurements also decreased from 3.56(±5.77) g CO_2 m^{-2} d^{-1} to 2.78(±5.02) g CO_2 m^{-2} d^{-1} using LCfrac, compared with 3.28(±1.49) g CO_2 m^{-2} d^{-1} using MRD'_F. These findings clearly show the improvement in modeled grid NEP as a result of correcting the representativeness of the EC flux measurements.

The uncertainty of modeled grid NEP based on the EC tower measurements with poor representativeness was reduced by the upscaling process proposed in this study. For the EC04 tower with the lowest representativeness, the MD of the modeled NEP at the grid scale using the corrected EC04 NEP measurements decreased from 23.7(±3.6) g CO_2 m^{-2} d^{-1} to 20.42(±2.78) g CO_2 m^{-2} d^{-1} using LCfrac and 5.57(±1.53) g CO_2 m^{-2} d^{-1} using MRD'_F. However, the effect of over-correction was observed in some cases when using MRD'_F, especially for EC towers with high representativeness. For example, for the EC05 tower with the highest representativeness, the MD decreased from 0.47(±0.33) g CO_2 m^{-2} d^{-1} to 0.43(±0.19) g CO_2 m^{-2} d^{-1} using LCfrac but increased to 1.57(±0.38) g CO_2 m^{-2} d^{-1} using MRD'_F. This is consistent with the findings of the previous section. This over-correction can be quantified using a reduced MD (the difference in the mean MD of the modeled grid NEP of the 17 sites and the corresponding mean grid NEP between the original and corrected EC measurements), as shown in Figure 7. The corrected EC measurements using LCfrac and MRD'_F differed; this is related to the representativeness of the EC towers (i.e., the MRD). For EC towers with lower representativeness (larger absolute value of MRD), such as EC04, EC01, EC17, EC13, and EC10, MRD'_F produced the best correction, but may also result in a negative reduced MD, i.e., an opposite effect for small MRD EC measurements (Figure 7). Although the reduced MD using LCfrac was smaller than that using MRD'_F, the negative effect using LCfrac was also small. Therefore, for EC NEP measurements with an MRD greater than 45%, i.e., LCfrac and DMEVI larger than 10%, the best correction can be achieved with MRD'_F and MRD'_E, and 80% of the MRD can be removed. For EC measurements with an MRD between 20% and 45% (LCfrac and DMEVI between 5% and 10%), the best correction can be achieved using LCfrac and DMEVI, and 20% of the MRD can be removed. For EC measurements with an MRD smaller than 20% (LCfrac and DMEVI smaller than 5%), the MRD cannot be corrected due to various uncertainties.

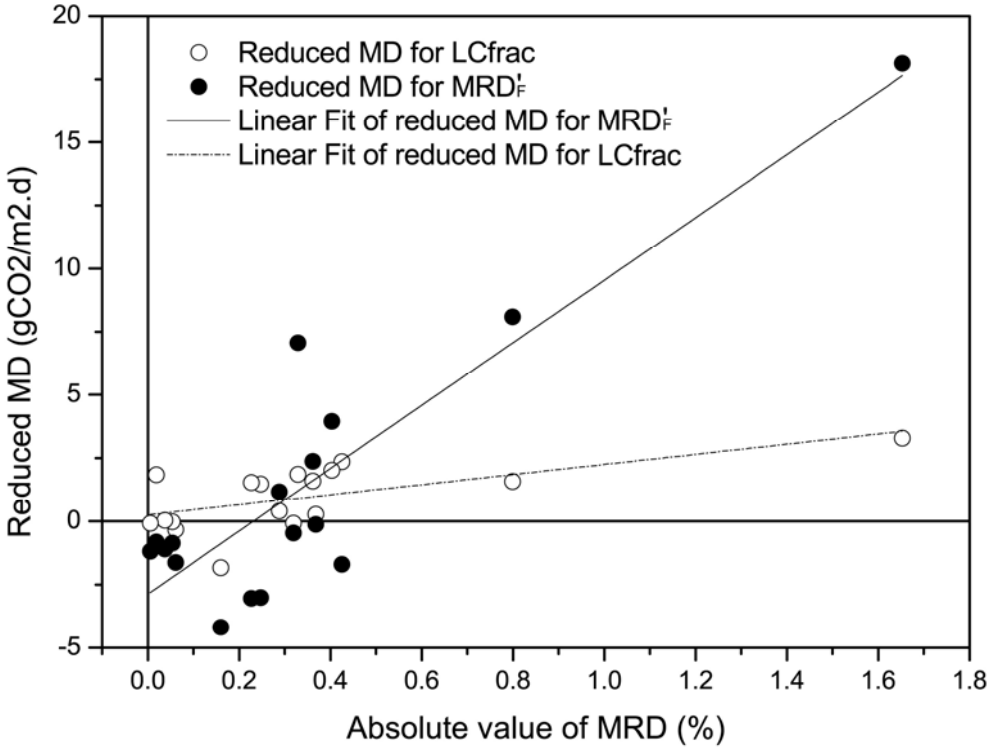

Figure 7. Effect of improved representativeness of EC measurements for modeling grid-scale NEP using the model-data fusion method.

5 Summary and Conclusions

We evaluate the representativeness of eddy covariance (EC) flux towers for grid scale (5 km × 5 km in this study) NEP of an agricultural landscape in northwestern China based on HiWATER-MUSOEXE. An EC flux observation matrix including 17 EC towers within the study site was used to test the effect of spatial representativeness and uncertainty of EC tower flux measurements on grid-scale NEP modeling using a model-data fusion method that integrated remote sensing data and footprint model results. We found that: (1) The temporal and spatial variability of NEP was dominated by the variability in GPP as well as by landscape fragmentation of the land cover type within the footprints. The significant surface heterogeneity led to a large systematic error when using a single EC tower to monitor long-term NEP changes at the grid scale. The overestimation of NEP may exceed 40(±33)% even if the tower appears to be located within a dominant underlying surface of the study area. (2) Even if there are 17 EC towers within a 5 km × 5 km area, their arithmetic mean cannot represent the mean NEP at the grid scale because the land cover structure within the tower footprint area is biased. The bias is significant with a mean difference of approximately 5.9 g CO_2 m^{-2} d^{-1}. This suggests that EC measurements should be upscaled to the corresponding grid scale before using them to validate NEP products from satellite imagery or biogeochemical models. (3) The systematic bias of EC measurements should be corrected before upscaling using a data-model fusion approach. Alternatively, most of the systematic bias may be propagated to the grid scale due to the scale dependence of the model parameters. (4) A systematic bias of EC measurements greater than 20% can be corrected using the four indicators proposed in this study. These include the difference in the mean EVI (DMEVI) and fraction of land cover type (LCfrac) between the footprint area of the EC tower and the grid area, the estimated MRD based on DMEVI, and the estimated mean relative difference (MRD) based on LCfrac.

The findings of this study suggest that the parameters of both remote sensing-based models and

biogeochemical models calibrated by EC measurements with low spatial representativeness exhibit scale mismatch with pixel or model grid. The scale mismatch parameters may lead to a large systematic error in estimated grid-scale NEP. The temporal-spatial variability and scale dependency of model parameters require a strong parameterization scheme to improve the accuracy of NEP modeling. If the measurement of pure NEP for a specific land cover type is available, the fraction of land cover type based on high-resolution land cover mapping or the fraction of vegetation cover has potential to be combined into a parameterization scheme of a remote sensing-based model, such as VPRM, to correct the bias associated with NEP modeling. This also will benefit from finer spatial resolution land cover mapping, such as the global land cover map that is already available at a 30-m resolution (Ran and Li, 2015), or a higher resolution land cover dataset in the future.

Acknowledgments:

This study was supported by National Science Foundation of China projects (grant number: 41471359, 91425303), the CAS Interdisciplinary Innovation Team of the Chinese Academy of Sciences, and Youth Innovation Promotion Association of Chinese Academy of Sciences (Grant number: 2016375). We thank the editor and two anonymous reviewers for their extremely helpful comments on this paper.

References

Anderson, M.C., Kustas, W.P., Alfieri, J.G., Gao, F., Hain, C., Prueger, J.H., Evett, S., Colaizzi, P., Howell, T., Chávez, J.L., 2012. Mapping daily evapotranspiration at landsat spatial scales during the BEAREX'08 field campaign. Adv. Water Resour. 50, 162-177. doi:10.1016/j.advwatres.2012.06.005.

Baldocchi, D., Ma, S., 2013. How will land use affect air temperature in the surface boundary layer? Lessons learned from a comparative study on the energy balance of an oak savanna and annual grassland in California, USA. Tellus B 65, 19994. doi:10.3402/tellusb.v65i0.19994.

Ballantyne, A.P., Alden,C.B., Miller, J.B., Tans, P.P., White, J.W., 2012. Increase in observed net carbon dioxide uptake by land and oceans during the past 50 years. Nature 488, 70-72. doi:10.1038/nature11299.

Barcza, Z., Kern, A., Haszpra, L., Kljun, N., 2009. Spatial representativeness of tall tower eddy covariance measurements using remote sensing and footprint analysis. Agric. Forest Meteorol. 149, 795-807. doi:10.1016/j.agrformet.2008.10.021.

Beyrich, F., Mengelkamp, H., 2006. Evaporation over a heterogeneous land surface: EVA_GRIPS and the LITFASS-2003 experiment—an overview. Boundary-Layer Meteorol. 121, 5-32. doi:10.1007/s10546-006-9079-z.

Blanken, P.D., Black, T.A., Neumann, H.H., Hartog, G.d, Yang, P.C., Nesic, Z., Staebler, R., Chen, W., Novak, M.D., 1998. Turbulence flux measurements above and below the overstory of a boreal aspen forest. Boundary-Layer Meteorol. 89, 109–140. doi:10.1023/A:1001557022310.

Boles, S.H., Xiao, X., Liu, J., Zhang, Q., Munkhtuya, S., Chen, S., Ojima, D., 2004. Land cover characterization of temperate East Asia using multi-temporal VEGETATION sensor data. Remote Sens. Environ. 90, 477– 489. doi:10.1016/j.rse.2004.01.016.

Borken, W., Matzner, E., 2009. Reappraisal of drying and wetting effects on C and N mineralization and fluxes in soils. Glob. Change Biol. 15, 808-824. doi:10.1111/j.1365-2486.2008.01681.x.

Burba, G., 2013. Eddy Covariance Method for Scientific, Industrial, Agricultural, and Regulatory Applications: A Field Book on Measuring Ecosystem Gas Exchange and Areal Emission Rates. LI-COR Biosciences, Lincoln, NE.

Burba, G.G., 2001. Illustration of flux footprint estimates affected by measurement height, surface roughness and thermal stability, in: Hubbard, K.G., Sivakumar, M.V.K. (Eds.), Automated Weather Stations for Applications in Agriculture and Water Resources Management: Current

Use and Future Perspectives. World Meteorological Organization, Geneva, Switzerland, pp. 77-87.

Chasmer, L., Barr, A., Hopkinson, C., McCaughey, H., Treitz, P., Black, A., Shashkov, A., 2009. Scaling and assessment of GPP from MODIS using a combination of airborne lidar and eddy covariance measurements over jack pine forests. Remote Sens. Environ. 113, 82-93. doi:10.1016/j.rse.2008.08.009.

Chasmer, L., Kljun, N., Hopkinson, C., Brown, S., Milne, T., Giroux, K., Barr, A., Devito, K., Creed, I., Petrone, R., 2011. Characterizing vegetation structural and topographic characteristics sampled by eddy covariance within two mature aspen stands using lidar and a flux footprint model: scaling to MODIS. J. Geophys. Res. 116. doi:10.1029/2010jg001567.

Chen, B., Black, T.A., Coops, N.C., Hilker, T., Trofymow, J.A., Morgenstern, K., 2009. Assessing tower flux footprint climatology and scaling between remotely sensed and eddy covariance measurements. Boundary-Layer Meteorol. 130, 137-167. doi:10.1007/s10546-008-9339-1.

Chen, B., Ge, Q., Fu, D., Yu, G., Sun, X., Wang, S., Wang, H., 2010. A data-model fusion approach for upscaling gross ecosystem productivity to the landscape scale based on remote sensing and flux footprint modelling. Biogeosciences 7, 2943-2958. doi:10.5194/bg-7-2943-2010.

Chen, J., Zhu, X., Vogelmann, J.E., Gao, F., Jin, S., 2011. A simple and effective method for filling gaps in landsat ETM+ SLC-off images. Remote Sens. Environ. 115, 1053–1064. doi:10.1016/j.rse.2010.12.010.

Cheng, G., Li, X., Zhao, W., Xu, Z., Feng, Q., Xiao, S., Xiao, H., 2014. Integrated study of the water–ecosystem–economy in the Heihe River Basin. Natl. Sci. Rev. 1, 413-428. doi:10.1093/nsr/nwu017.

Coops, N., Black, T., Jassal, R., Trofymow, J., Morgenstern, K., 2007. Comparison of MODIS, eddy covariance determined and physiologically modelled gross primary production (GPP) in a Douglas-fir forest stand. Remote Sens. Environ. 107, 385-401. doi:10.1016/j.rse.2006.09.010.

Falge, E., Baldocchi, D., Olson, R., Anthoni, P., Aubinet, M., Bernhofer, C., Burba, G., Ceulemans, R., Clement, R., Dolman, H., Granier, A., Gross, P., Grünwald, T., Hollinger, D., Jensen, N., Katul, G., Keronen, P., Kowalski, A., Lai, C.T., Law, B.E., Meyers, T., Moncrieff, J., Moors, E., Munger, J.W., Pilegaard, K., Rannik,U¨ ., Rebmann, C., Suyker, A., Tenhunen, J., Tu, K., Verma, S., Vesala, T., Wilson, K., Wofsy, S., 2001. Gap filling strategies for defensible annual sums of net ecosystem exchange. Agric. Forest Meteorol. 107, 43-69. doi:10.1016/S0168-1923(00)00225-2.

Foken, T., Wichura, B., 1996. Tools for quality assessment of surface-based flux measurements. Agric. Forest Meteorol. 78, 83-105. doi:10.1016/0168-1923(95)02248-1.

Göckede, M., Foken, T., Aubinet, M., Aurela, M., Banza, J., Bernhofer, C., Bonnefond, J.M., Brunet, Y., Carrara, A., Clement, R., Dellwik, E., Elbers, J., Eugster, W., Fuhrer, J., Granier, A. Grünwald, T., Heinesch, B., Janssens, I. A., Knohl, A., Koeble, R., Laurila, T., Longdoz, B., Manca, G., Marek, M., Markkanen, T., Mateus, J., Matteucci, G., Mauder, M., Migliavacca, M., Minerbi, S., Moncrieff, J., Montagnani, L., Moors, E., Ourcival, J.-M., Papale, D., Pereira, J., Pilegaard, K., Pita, G., Rambal, S., Rebmann, C., Rodrigues, A., Rotenberg, E., Sanz, M. J., Sedlak, P., Seufert, G., Siebicke, L., Soussana, J. F., Valentini, R., Vesala, T., Verbeeck, H., Yakir, D., 2008. Quality control of CarboEurope flux data–Part 1: Coupling footprint analyses with flux data quality assessment to evaluate sites in forest ecosystems. Biogeosciences, 5, 433-450.

Göckede, M., Michalak, A.M., Vickers, D., Turner, D.P., Law, B.E., 2010. Atmospheric inverse modeling to constrain regional-scale CO2 budgets at high spatial and temporal resolution. J. Geophys. Res. Atmos. 115. doi:10.1029/2009JD012257.

Grimmond, C.S.B., Oke, T.R., 1999. Evapotranspiration rates in urban areas, in: Ellis, B. (Ed.), Impacts of Urban Growth on Surface Water and Groundwater Quality. IAHS Publications, Oxford, UK, pp. 235–243.

Heinsch, F.A., Zhao, M.S., Running, S.W., Kimball, J.S., Nemani, R.R., Davis, K.J., Bolstad, P.V., Cook, B.D., Desai, A.R., Ricciuto, D.M., Law, B.E., Oechel, W.C., Kwon, H., Luo, H.Y., Wofsy, S.C., Dunn, A.L., Munger, J.W., Baldocchi, D.D., Xu, L.K., Hollinger, D.Y., Richardson, A.D., Stoy, P.C., Siqueira, M.B.S., Monson, R.K., Burns, S.P., Flanagan, L.B., 2006. Evaluation of remote sensing based terrestrial productivity from MODIS using regional tower eddy flux network observations. IEEE Trans. Geosci. Remote Sens. 44, 1908–1925. doi:10.1109/TGRS.2005.853936.

Højstrup, J., 1993. A statistical data screening procedure. Meas. Sci. Technol. 4, 153–157. doi:10.1088/0957-0233/4/2/003.

Huete, A., Liu, H.O., Batchily, K., Leeuwen, W.V., 1997. A comparison of vegetation indices over a global set of TM images for EOS-MODIS. Remote Sens. Environ. 59, 440– 451. doi:10.1016/S0034-4257(96)00112-5.

Huntzinger, D.N., Post, W.M., Wei, Y., Michalak, A.M., West, T.O., Jacobson, A.R., Baker, I.T., Chen, J.M., Davis, K.J., Hayes, D.J., Hoffman, F.M., Jain, A.K., Liu, S., McGuire, A.D., Neilson, R.P., Potter, C., Poulter, B., Price, D., Raczka, B.M., Tian, H.Q., Thornton, P., Tomelleri, E., Viovy, N., Xiao, J., Yuan, W., Zeng, N., Zhao, M., Cook, R., 2012. North American Carbon Program (NACP) regional interim synthesis: terrestrial biospheric model intercomparison. Ecol. Modell. 232, 144-157. doi:10.1016/j.ecolmodel.2012.02.004.

Intergovernmental Panel of Climate Change (IPCC), 2013. Working group I contribution to the IPCC 5th assessment report. Climate change 2013: the physical science basis. Final draft underlying scientific-technical assessment. http://www.climatechange2013.org/images/uploads/WGIAR5_WGI-12Doc2b_FinalDraft_All.pdf (accessed 2015.05.03).

Jabro, J.D., Sainju, U., Stevens, W.B., Evans, R.G., 2008. Carbon dioxide flux as affected by tillage and irrigation in soil converted from perennial forages to annual crops. J. Environ. Manag. 88, 1478-1484. doi:10.1016/j.jenvman.2007.07.012.

Jacobs, J., Mohanty, B.P., Hsu, E., Miller, D., 2004. SMEX02: Field scale variability, time stability and similarity of soil moisture. Remote Sens. Environ. 92, 436–446. doi:10.1016/j.rse.2004.02.017.

Kaimal, J.C., Finnigan, J.J., 1994. Atmos. Bound. Layer Flows Oxford University Press, New York.

Kimball, J.S., Jones, L.A., Zhang, K., Heinsch, F.A., McDonald, K.C., Oechel, W.C., 2009. A satellite approach to estimate land-atmosphere CO2 exchange for boreal and Arctic biomes using MODIS and AMSR-E. IEEE Trans. Geosci. Remote Sens. 47, 569-587. doi:10.1109/TGRS.2008.2003248.

Kljun, N., Calanca, P., Rotach, M.W., Schmid, H.P., 2004. A simple parameterisation for flux footprint predictions. Boundary-Layer Meteorol. 112, 503-523. doi:10.1023/B:BOUN.0000030653.71031.96.

Kljun, N., Calanca, P., Rotach, M.W., Schmid, H.P., 2015. A simple two-dimensional parameterisation for Flux footprint prediction (FFP). Geosci. Model. Dev. 8, 3695-3713. doi:10.5194/gmd-8-3695-2015.

Kljun, N., Rotach, M.W., Schmid, H.P., 2002. A three-dimensional backward Lagrangian footprint model for a wide range of boundary-layer stratifications. Boundary-Layer Meteorol. 103, 205-226. doi:10.1023/A:1014556300021.

Kreba, S.A., Coyne, M.S., McCulley, R.L., Wendroth, O.O., 2013. Spatial and temporal patterns of carbon dioxide flux in crop and grass land-use systems. Vadose Zone J. 12. doi:10.2136/vzj2013.01.0005.

Kwon, Y., Larsen, C.P.S., 2012. Use of pixel- and plot-scale screening variables to validate MODIS GPP predictions with Forest Inventory and Analysis NPP measures across the eastern USA. Int. J. Remote Sens. 33, 6122-6148. doi:10.1080/01431161.2012.680615.

Lasslop, G., Reichstein, M., Kattge, J., Papale, D., 2008. Influences of observation errors in eddy flux data on inverse model parameter estimation. Biogeosciences 5, 1311–1324. doi:10.5194/bg-5-1311-2008.

Li, S., Zhao, W., 2010. Satellite-based actual evapotranspiration estimation in the middle reach of the Heihe River Basin using the SEBAL method. Hydrol. Process. 24, 3337-3344. doi:10.1002/hyp.7748.

Li, X., 2014. Characterization, controlling, and reduction of uncertainties in the modeling and observation of land-surface systems. Sci. China Earth Sci. 57, 80-87. doi:10.1007/s11430-013-4728-9.

Li, X., Cheng, G., Liu, S., Xiao, Q., Ma, M., Jin, R., Che, T., Liu, Q., Wang, W., Qi, Y., Wen, J., Li, H., Zhu, G., Guo, J., Ran, Y., Wang, S., Zhu, Z., Zhou, J., Hu, X., Xu, Z., 2013. Heihe watershed allied telemetry experimental Research (HiWATER): scientific objectives and experimental design. Bull. Am. Meteorol. Soc. 94, 1145-1160. doi:10.1175/BAMS-D-12-00154.1.

Liu, S.M., Xu, Z.W., Song, L.S., Zhao, Q.Y., Ge, Y., Xu, T.R., Ma, Y.F., Zhu, Z.L., Jia, Z.Z., Zhang, F., 2016. Upscaling evapotranspiration measurements from multi-site to the satellite pixel scale over heterogeneous land surfaces. Agric. Forest Meteorol. doi:10.1016/j.agrformet.2016.04.008.

Liu, S.M., Xu, Z.W., Wang, W.Z., Jia, Z.Z., Zhu, M.J., Bai, J., Wang, J.M., 2011. A comparison of eddy-covariance and large aperture scintillometer measurements with respect to the energy balance closure problem. Hydrol. Earth Syst. Sci. 15, 1291-1306. doi:10.5194/hess-15-1291-2011.

Liu, X., Bo, Y., 2015. Object-based crop species classification based on the combination of airborne hyperspectral images and LiDAR data. Remote Sens. 7, 922-950. doi:10.3390/rs70100922.

Lloyd, J., Taylor, J.A., 1994. On the temperature dependence of soil respiration. Funct. Ecol. 8, 315-323. doi:10.2307/2389824.

Luo, Y., Ogle, K., Tucker, C., Fei, S., Gao, C., LaDeau, S., Clark, J.S., Schimel, D.S., 2011. Ecological forecasting and data assimilation in a data-rich era. Ecol. Appl. 21, 1429-1442. doi:10.1890/09-1275.1.

Mahadevan, P., Wofsy, S.C., Matross, D.M., Xiao, X., Dunn, A.L., Lin, J.C., Gerbig, C., Munger, J.W., Chow, V.Y., Gottlieb, E.W., 2008. A satellite-based biosphere parameterization for net ecosystem CO2 exchange: vegetation photosynthesis and respiration model (VPRM). Glob. Biogeochem. Cycles 22. doi:10.1029/2006gb002735.

McMillen, R.T., 1988. An eddy correlation technique with extended applicability to non-simple terrain. Boundary-Layer Meteorol. 43, 231-245. doi:10.1007/BF00128405.

Mitchell, S., Beven, K., Freer, J., 2009. Multiple sources of predictive uncertainty in modeled estimates of net ecosystem CO2 exchange. Ecol. Modell. 220, 3259-3270. doi:10.1016/j.ecolmodel.2009.08.021.

Moore, C.J., 1986. Frequency response corrections for eddy correlation systems. Boundary-Layer Meteorol. 37, 17-35. doi:10.1007/BF00122754.

Poulos, G.S., Blumen, W., Fritts, D.C., Lundquist, J.K., Sun, J., Burns, S.P., Nappo, C., Banta, R., Newsom, R., Cuxart, J., Terradellas, E., Balsley, B., Jensen, M., 2002. CASES-99: A comprehensive investigation of the stable nocturnal boundary layer. Bull. Am. Meteorol. Soc. 83, 555-581. doi:10.1175/1520-0477(2002)083<0555:CACIOT>2.3.CO;2.

Raich, J.W., Rastetter, E.B., Melillo, J.M., Kicklighter, D.W., Steudler, P.A., Peterson, B.J., Grace, A.L., Moore III, B., Vorosmarty, C.J., 1991. Potential net primary productivity in South America: application of a global model. Ecol. Appl. 1, 399– 429. doi:10.2307/1941899.

Ran, Y., Li, X., 2015. First comprehensive fine-resolution global land cover map in the world from China—comments on global land cover map at 30-m resolution. Sci. China Earth Sci. 58, 1677-1678. doi:10.1007/s11430-015-5132-4.

Randerson, J.T., Hoffman, F.M., Thornton, P.E., Mahowald, N.M., Lindsay, K., Lee, Y., Nevison, C.D., Doney, S.C., Bonan, G., Stöckli, R., Covey, C., Running, S.W., Fung, I.Y., 2009. Systematic assessment of terrestrial biogeochemistry in coupled climate-carbon models. Glob. Change Biol. 15, 2462–2484. doi:10.1111/j.1365-2486.2009.01912.x.

Raupach, M.R., Rayner, P.J., Barrett, D.J., DeFries, R.S., Heimann, M., Ojima, D.S., Quegan, S., Schmullius, C.C., 2005. Model-data synthesis in terrestrial carbon observation: methods, data

requirements and data uncertainty specifications. Glob. Change Biol. 11, 378-397. doi:10.1111/j.1365-2486.2005.00917.x.

Sasai, T., Saigusa, N., Nasahara, K.N., Ito, A., Hashimoto, H., Nemani, R., Hirata, R., Ichii, K., Takagi, K., Saitoh, T.M., Ohta, T., Murakami, K., Yamaguchi, Y., Oikawa, T., 2011. Satellite-driven estimation of terrestrial carbon flux over Far East Asia with 1-km grid resolution. Remote Sens. Environ. 115, 1758-1771. doi:10.1016/j.rse.2011.03.007.

Schneider, K., Huisman, J.A., Breuer, L., Zhao, Y., Frede, H.G., 2008. Temporal stability of soil moisture in various semi-arid steppe ecosystems and its application in remote sensing. J. Hydrol. 359, 16-29. doi:10.1016/j.jhydrol.2008.06.016.

Schotanus, P., Nieuwstadt, F.T.M., De Bruin, H.A.R., 1983. Temperature measurement with a sonic anemometer and its application to heat and moisture fluxes. Boundary-Layer Meteorol. 26, 81-93. doi:10.1007/BF00164332.

Sellers, P., Hall, F., Ranson, K.J., Margolis, H., Kelly, B., Baldocchi, D., den Hartog, G., Cihlar, J., Ryan, M.G., Goodison, B., Crill, P., Lettenmaier, D., Wickland, D.E., 1995. The Boreal Ecosystem-Atmosphere Study (BOREAS): an overview and early results from the 1994 field year. Bull. Am. Meteorol. Soc. 76, 1549-1577. doi:10.1175/1520-0477(1995)076<1549:TBESAO>2.0.CO;2.

Jin, R., Li, X., Yan, B.P., Li, X.H., Luo, W.M., Ma, M.G., Guo, J.W., Kang, J., Zhu, Z.L., Zhao, S., 2014. A nested ecohydrological wireless sensor network for capturing the surface heterogeneity in the midstream areas of the Heihe River Basin, China. IEEE Geosci. Remote Sens. Lett. 11, 2015-2019. doi:10.1109/LGRS.2014.2319085.

Turner, D.P., Ritts, W.D., Cohen, W.B., Gower, S.T., Running, S.W., Zhao, M., Costa, M.H., Kirschbaum, A.A., Ham, J.M., Saleska, S.R., Ahl, D.E., 2006. Evaluation of MODIS NPP and GPP products across multiple biomes. Remote Sens. Environ. 102, 282-292. doi:10.1016/j.rse.2006.02.017.

Twine, T.E., Kustas, W.P., Norman, J.M., Cook, D.R., Houser, P.R., Meyers, T.P., Prueger, J.H., Starks, P.J., Wesely, M.L., 2000. Correcting eddy-covariance flux underestimates over a grassland. Agric. Forest Meteorol. 103, 279-300. doi:10.1016/S0168-1923(00)00123-4.

Vachaud, G., Passerat De Silans, A., Balabanis, P., Vauclin, M., 1985. Temporal stability of spatially measured soil water probability density function. Soil Sci. Soc. Am. J. 49, 822-828. doi:10.2136/sssaj1985.03615995004900040006x.

Verma, M., Friedl, M.A., Richardson, A.D., Kiely, G., Cescatti, A., Law, B.E., Wohlfahrt, G., Gielen, B., Roupsard, O., Moors, E.J., Toscano, P., Vaccari, F.P., Gianelle, D., Bohrer, G., Varlagin, A., Buchmann, N., van Gorsel, E., Montagnani, L., Propastin, P., 2014. Remote sensing of annual terrestrial gross primary productivity from MODIS: an assessment using the FLUXNET la Thuile data set. Biogeosciences 11, 2185–2200. doi:10.5194/bg-11-2185-2014.

Wang, J.M., Zhuang, J.X., Wang, W.Z., Liu, S.M., Xu, Z.W., 2015. Assessment of uncertainties in eddy covariance flux measurement based on very intensive flux matrix of HiWATER-MUSOEXE. IEEE Geosci. Remote Sens. Lett. 12, 259-263.

Wang, Y., Trudinger, C.M., Enting, I.G., 2009. A review of applications of model–data fusion to studies of terrestrial carbon fluxes at different scales. Agric. Forest Meteorol. 149, 1829-1842. doi:10.1016/j.agrformet.2009.07.009.

Webb, E.K., Pearman, G.I., Leuning, R., 1980. Correction of the flux measurements for density effects due to heat and water vapour transfer. Q. J. Roy. Meteorol. Soc. 106, 85–100. doi:10.1002/qj.49710644707.

Weckwerth, T.M., Parsons, D.B., Koch, S.E., Moore, J.A., LeMone, M.A., Demoz, B.B., Flamant, C., Geerts, B., Wang, J., Feltz, W.F., 2004. An overview of the International H2O Project (IHOP_2002) and some preliminary highlights. Bull. Am. Meteorol. Soc. 85, 253-277. doi:10.1175/BAMS-85-2-253.

Weng, E., Luo, Y., Gao, C., Oren, R., 2011. Uncertainty analysis of forest carbon sink forecast with varying measurement errors: a data assimilation approach. J. Plant Ecol. 4, 178-191. doi:10.1093/jpe/rtr018.

Wilczak, J.M., Oncley, S.P., Stage, S.A., 2001. Sonic anemometer tilt correction algorithms. Boundary-Layer Meteorol. 99, 127-150. doi:10.1023/A:1018966204465.

Xiao, J., Davis, K.J., Urban, N.M., Keller, K., Saliendra, N.Z., 2011. Upscaling carbon fluxes from towers to the regional scale: influence of parameter variability and land cover representation on regional flux estimates. J. Geophys. Res. Biogeosci. 116. doi:10.1029/2010jg001568.

Xiao, X., Hollinger, D., Aber, J., Goltz, M., Davidson, E.A., Zhang, Q., Moore, B., 2004a. Satellite-based modeling of gross primary production in an evergreen needleleaf forest. Remote Sens. Environ. 89, 519–534. doi:10.1016/j.rse.2003.11.008.

Xiao, X., Zhang, Q., Braswell, B., Urbanski, S., Boles, S., Wofsy, S.C., Moore III, B., Ojima, D., 2004b. Modeling gross primary production of temperate deciduous broadleaf forest using satellite images and climate data. Remote Sens. Environ. 91, 256– 270. doi:10.1016/j.rse.2004.03.010.

Xu, Z., Liu, S., Li, X., Shi, S., Wang, J., Zhu, Z., Xu, T., Wang, W., Ma, M., 2013. Intercomparison of surface energy flux measurement systems used during the HiWATER-MUSOEXE. J. Geophys. Res. Atmos. 118, 13140-13157. doi:10.1002/2013JD020260.

Zhang, F., Chen, J.M., Chen, J., Gough, C.M., Martin, T.A., Dragoni, D., 2012. Evaluating spatial and temporal patterns of MODIS GPP over the conterminous U.S. against flux measurements and a process model. Remote Sens. Environ. 124, 717-729. doi:10.1016/j.rse.2012.06.023.

Zhang, L., Sun, R., Xu, Z., Qiao, C., Jiang, G., 2015. Diurnal and seasonal variations in carbon dioxide exchange in ecosystems in the Zhangye Oasis area, Northwest China. PLOS ONE 10, e0120660. doi:10.1371/journal.pone.0120660.

Zhu, X., Chen, J., Gao, F., Chen, X., Masek, J.G., 2010. An enhanced spatial and temporal adaptive reflectance fusion model for complex heterogeneous regions. Remote Sens. Environ. 114, 2610-2623. doi:10.1016/j.rse.2010.05.032.